J. Fluid Mech. (2005), *vol.* 538, *pp.* 245–267.
doi:10.1017/S0022112005005434 Printed in the United Kingdom

Mixing regimes for the flow of dense fluid down slopes into stratified environments

By PETER G. BAINES

Department of Civil and Environmental Engineering, University of Melbourne, Australia 3010
and School of Mathematics, University of Bristol, Bristol BS8 1TW, UK

(Received 8 July 2004 and in revised form 4 March 2005)

Downslope flows into density-stratified environments have been observed to have the character of detraining gravity currents on small slopes, and of entraining plumes on steep slopes. In this paper, observations of flows on slopes of intermediate (20°–30°) steepness are described, and their mixing properties quantified. Both gravity-current-like and plume-like flows are observed, and an observational boundary between these two types is identified. Theoretical models for the bulk properties of these flows are presented, and their predictions are compared with the observations. A theoretical criterion is derived for the limit of applicability of the gravity-current model in terms of the Buoyancy number, the bottom slope and the bottom drag coefficient. This provides a criterion for the boundary between the plume-like and gravity-current-like flows, which is consistent with the observations. These results have implications for the modelling of downslope flows in nature, and indicate where the appropriate dynamical model may change from one type to the other.

1. Introduction

The nature of mixing in downslope flows into stratified environments is important for the dynamics of nocturnal flows on sloping terrain in the atmosphere, and of dense overflows in the ocean (Price & Baringer 1994; Nielsen, Pratt & Helfrich 2004). Experimental studies of the flow of dense fluid down slopes into density-stratified environments have been described for the case of small (12° and less) slopes in Baines (2001*a*) and for vertical (90°) slopes in Baines (2002). In the case of small slopes, the flow has the character of gravity currents, and detrains fluid continuously to the environment along its path down to the level of neutral density, where it leaves the slope in the form of an intrusion. On a point of terminology, the terms 'gravity current' and 'density current' are used interchangeably in the literature; the term 'gravity current' is chosen here. With vertical slopes, on the other hand, the flow has the character of turbulent plumes. In the stratified environment, these plumes entrain environmental fluid into them along their path, overshoot the equilibrium level of neutral density, and then return to it in a large-scale motion termed 'springback'. Theoretical models for the bulk properties of these flows, including mixing and entrainment, were presented and compared with the experiments. The study reported here investigates downslope flows for the ranges of parameter values that lie in between these two extreme situations, using the same techniques as in the previous studies. Nearly all the experiments described here are for slope angles between 20° and 30°, and both flow types were observed over this range of slope angles. Between these two types there is a transitional range, as described here. Experiments have also

been performed with increased roughness on the sloping bottom, and this is found to affect the flow type.

The plan of the paper is as follows. The experimental set-up and the runs carried out are briefly described in § 2, and the quantitative observations and descriptions of the flows are presented in § 3. The theoretical model for flow in the plume or P-regime is discussed and compared with observations in § 4, and similarly for flows in the gravity current or GC-regime in § 5. The boundary in parameter space between these two regimes is described in § 6, and the conclusions are summarized in § 7. An early version of some of these results was presented in Baines (2001*b*).

There is no need to summarize the details of the pure gravity current and plume flows, since they are given in Baines (2001*a*, 2002), but the basic scaling is repeated here for later convenience. In any experimental downflow with a constant supply of uniformly dense fluid into a uniformly stratified environment, the principal given parameters are the initial volume inflow rate Q_0 and buoyancy G_0, and the buoyancy frequency of the environment, N. The local parameters Q and G also specify the state of the flow at subsequent positions. Here, we assume that the flow is uniform across the slope (i.e. in the y-direction), so that the properties are two-dimensional in the mean. The parameters $G$and N are given by

$$G = g'(z) = \frac{g\Delta\rho(z)}{\bar{\rho}_0}, \quad N^2 = -\frac{g}{\bar{\rho}_0}\frac{\mathrm{d}\rho_0(z)}{\mathrm{d}z}, \tag{1.1}$$

where z is the vertical coordinate, g is the acceleration due to gravity, ρ_0 is the undisturbed environmental density profile with $\bar{\rho}_0$ a mean value, and $\Delta\rho$ is the local difference between density of the fluid in the downflow and the environment. From Q and G we may define a length scale L and time scale τ by

$$L = \left(\frac{Q^2}{G}\right)^{1/3}, \quad \tau = \left(\frac{Q}{G^2}\right)^{1/3}. \tag{1.2}$$

L may be approximately identified with the thickness of the current, $\bar{d}$ (strictly, $\bar{d} = (R_i)^{1/3}L$, where Ri is defined by (1.5)). The scale speed is then $(QG)^{1/3} = L/\tau \approx (G\bar{d})^{1/2}$. The principal dimensionless parameter that can be formed from these quantities is B, the *buoyancy number* of the downflow, defined as

$$B \equiv \frac{QN^3}{G^2} = (N\tau)^3 \approx \left(\frac{\bar{d}}{D_s}\right)^{3/2}, \tag{1.3}$$

where D_s denotes the local vertical distance above the level where the environmental density is equal to the local mean density of the fluid in the downflow (the parameter B was termed M in Baines (2001*a*); the change was prompted by a referee who suggested that a suitable name be given to this parameter, now known as the buoyancy number). The value of B varies with position down the slope. At the top of the slope, where $Q = Q_0$ and $G = G_0$, $D_s = D \equiv G_0/N^2$, and

$$B = B_0 \equiv Q_0N^3/G_0^2. \tag{1.4}$$

B_0 is taken to be the principal parameter that characterizes each experimental run. If B is small, the time scale τ is small compared with the buoyancy period, and the thickness of the downflow is small compared with the vertical distance of travel. Values of B of order unity and larger are unrealistic for these flows, as the current thickness would be of the same order as its vertical length of flow for such values. Hence, $B \ll 1$ for most runs.

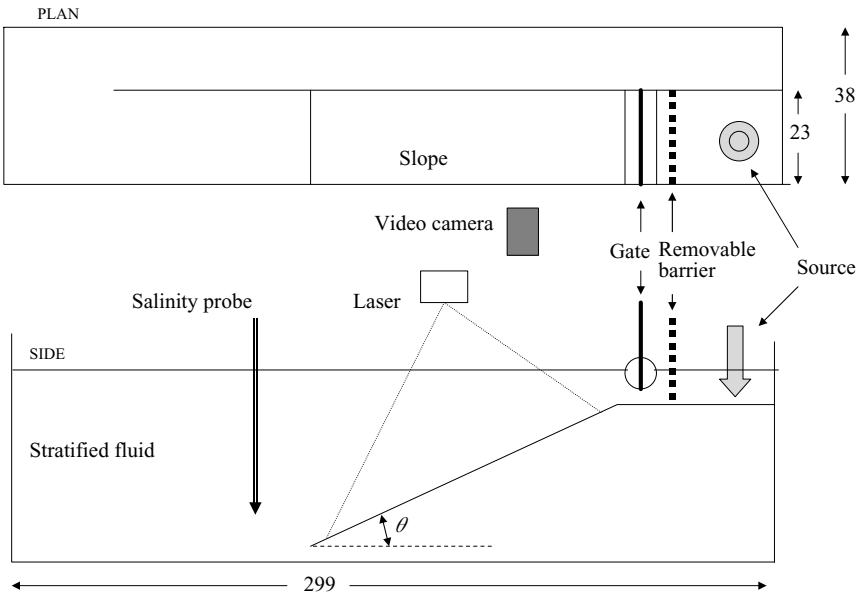

FIGURE 1. Plan and side views of the tank used in these experiments. A central vertical section of the flow on the slope was illuminated by a thin sheet of laser light from above, and video-recorded by viewing from the side. Only part of the total width of the tank was used, which enables the simulation of an effectively longer tank for these experiments. All measurements are in cm.

The other dimensionless parameters of relevance are the slope angle θ, the Reynolds number Re and Richardson number Ri, given by

$$Re = \frac{Q}{\nu}, \quad Ri = \frac{g'\bar{d}^3 \cos\theta}{Q^2}. \tag{1.5}$$

If the Reynolds number is sufficiently large (say, > 300), the dependence of the flow on its value appears to be small. For these cases the value of Re is not considered in the subsequent analysis, but it does have a noticeable effect when values are small. The value of the Richardson number is not predetermined, since $\bar{d}$ is determined by the dynamics, and must be observed.

2. Experiments

The experiments were carried out in a glass-sided tank with the configuration shown in figure 1. This is a very similar set-up to that described by Baines (2001*a*). This tank was rectangular in cross-section, 80 cm high with internal dimensions of 299 cm in length and 38 cm in width, open at the top and with a solid horizontal bottom. The effective working length of the tank was extended by inserting a thin vertical Perspex partition, extending from one end to a point 25 cm short of the other end, and with a uniform gap of 23 cm on one side and 15 cm on the other. The main working region of the tank was in the wider region of width 23 cm, and the experiment was made two-dimensional in this region as far as possible. For the low-frequency motions and changes produced in the ambient stratification, the fluid behind the partition could be regarded as a two-dimenional extension of the working region. A horizontal platform or shelf 40 cm long with a plane downward sloping extension 2 m in length was

inserted at the closed end of this region. The height of the horizontal platform varied from 20 to 40 cm depending on the slope angle. Three slope angles were used for the experiments described here: 20°, 25° and 30° to the horizontal. A fixed sluice-type gate was placed at a distance of 39 cm from the endwall. This consisted of a vertical barrier terminated at its bottom by a horizontal cylinder of radius 2 cm, leaving a gap of (typically) 1 cm above the horizontal platform below. For the 20° and 25° slope experiments, the configuration was slightly different from the others.. Here, the topography used for 12° slope experiments was tilted to the desired angle (20° or 25°), which gave a sloping shelf region behind the gate with bottom slope 8° and 13°, respectively. Since the region behind the gate was effectively continuously filled with inflowing fluid during the experiments, this did not appear to cause significant differences from the expected results with a horizontal shelf.

Before each experiment, the tank was filled with stratified fluid to a level above this gap. This was produced by the familiar two-tank mixing procedure with salt water. This filled the whole tank including the region on the far side of the Perspex partition and the region underneath the slope and horizontal platform. The purpose of this was to have an approximately uniform stratification in the tank, by having a horizontal cross-sectional area that was uniform with height during filling. After filling, the gaps connecting the region beneath the slope and platform were closed and sealed, so that the fluid there was isolated and not involved in the subsequent experiment. After these gaps were closed and all motion due to filling had subsided, the vertical density profile was measured by a conductivity probe, constructed in house, that was calibrated at the top and bottom by samples measured in an Anton Paar densitometer. This profile was designated $\rho_0(z)$, with z positive upwards and the origin taken at the level of the platform of the source.

During the experiment, dense fluid was continuously supplied by a hose from an external reservoir to the region of the tank behind the sluice gate. The start-up procedure was as follows. First, a temporary barrier across the tank was inserted between the sluice gate and the endwall, as depicted in figure 1. Then, all ambient fluid between this temporary barrier and the endwall was removed by vacuum cleaner. The dense water supply from the hose was then turned on. When the surface of this dense fluid equalled that of the ambient fluid in the tank, the temporary barrier was removed, giving a sudden commencement at the removal time to the release of continuously supplied dense fluid. This fluid then flowed through the gap under the sluice barrier and down the slope.

The main experiment was performed by suddenly releasing dense fluid of density ρ_i at the top of the slope in the manner just described, into a stationary stratified environment. This inflow was continued at a constant rate that was set and monitored by a flow meter in the inflow hose, and lasted for a fixed time that depended on the flow rate and ranged between 2 and 6 min. Various values of the inflow rate, inflow density and initial density gradient were used in a variety of experiments for each slope angle, and the details of these are given in table 1, which contain values of the controlling parameters and some key observations. The inflowing fluid was dyed with fluorescein, and illuminated in a thin central vertical section down the slope by a scanned beam from an argon ion laser, which gave a clear picture of a vertical cross-section of the motion. This cross-section was recorded on video tape for at least part of most runs. Overall observations of flows for these moderately steep slopes showed a variety of flow types ranging from gravity-current-like to plume-like, with a broadly two-dimensional form. These flows had an initial head structure that increased in size with slope angle, as described by Britter & Linden (1980). The pattern of the flow

	B_0	Q_0	g'_0	N	D	Re	$\bar{d}$	Ri_0	T_r	Surface
(*a*)	0.0030	1.32	22.2	1.04	20.5	132	0.27	0.236	210	S
	0.0046	2.73	21.81	0.934	24.99	273	0.12	0.0047	120	S
	0.0069	3.44	17.19	0.843	24.19	344	0.21	0.0126	180	S
	0.0085	4.15	13.29	0.713	26.14	415	0.53	0.108	162	Sa
	0.0109	4.15	12.80	0.756	22.38	415	0.15	0.0024	163	S
	0.013	5.56	12.41	0.713	24.43	556	0.31	0.0112	104	S
	0.023	8.38	11.26	0.713	22.16	838	2	1.205	160	Sa
	0.0290	3.79	6.316	0.674	13.92	379	0.53	0.0615	180	S
	0.0295	9.83	11.93	0.755	20.94	983	1.13	0.167	178	S
	0.043	8.38	8.74	0.731	16.36	838	1.25	0.228	110	S
	0.0566	11.21	11.52	0.877	14.99	1121	–	–	135	S
	0.076	14.04	7.10	0.651	16.77	1404	–	–	105	S
(*b*)	0.004	2.73	26.26	1.008	25.85	273	0.57	0.282	200	Doormat
	0.0057	2.73	18.75	0.904	22.95	273	0.56	0.188	360	Doormat
	0.0074	4.15	21.03	0.927	24.5	415	0.55	0.085	180	Doormat
	0.0091	5.56	22.10	0.931	25.51	556	0.66	0.100	120	Doormat
	0.0158	8.38	20.19	0.919	23.91	838	0.84	0.0967	120	Doormat
	0.0288	8.38	9.23	0.665	20.88	838	0.67	0.0195	155	Doormat
	0.044	8.38	8.55	0.728	16.11	838	0.78	0.0314	138	Doormat
	0.0838	14.04	8.57	0.760	14.82	1404	1.25	0.057	42	Doormat
(*c*)	0.0032	2.73	22.67	0.849	31.42	273	1.05	0.675	181	S
	0.0036	2.73	17.0	0.726	32.25	273	0.67	0.622	311	S
	0.0054	4.15	21.52	0.845	30.17	415	1.27	1.256	122	S
	0.0079	6.97	18.54	0.730	34.76	697	1.25	3.19	122	S
	0.0080	6.27	21.33	0.837	30.43	627	0.92	2.319	120	S
	0.026	13.33	14.30	0.737	26.34	1333	2	0.383	95	S
	0.0262	10.5	15.84	0.857	21.56	1050	1.79	0.747	170	S
	0.045	13.33	12.80	0.756	22.38	1333	2.5	0.583	90	S
	0.0691	12.62	6.739	0.629	17.03	1262	3.2	1.019	90	S
(*d*)	0.0018	0.614	25.01	1.22	16.79	61.4	0.27	1.131	360	S
	0.0040	1.32	22.65172	1.161	16.79	132	0.61	2.55	360	S
	0.0047	1.32	18.39	1.061	16.33	132	0.51	1.212	240	S
	0.00606	1.67	17.35	0.718	33.66	507	0.73	2.19	120	S
	0.008	2.73	27.56	1.305	16.18	273.3	0.89	2.252	180	S
	0.0083	2.73	24.04	1.206	16.53	273.3	0.68	0.876	240	S
	0.0224	5.21	14.65	0.973	15.46	520.6	1.22	0.85	120	S
	0.0279	6.27	19.52	1.193	13.72	626.5	0.87	0.284	120	S
	0.0732	10.50	5.552	0.599	15.48	1050.4	1.67	0.203	90	S
	0.0938	11.21	12.71	1.105	10.4	1121	1.15	0.133	90	S

TABLE 1. Parameters for the experiments (see text for definitions), including the observed values of $\bar{d}$ and Ri_0. T_r denotes the run time in seconds. (*a*) 20° slope, S smooth surface, Sa sandpaper (*b*) 20° slope, doormat surface, (*c*) 25° slope, smooth surface, (*d*) 30° slope, smooth surface.

behind the head was steady in the mean for the remainder of the run, and is our main concern here.

The observations made during the experiments included (i) videotapes of the motion in the laser-scanned vertical section viewed from the side, from which measurements of properties such as the depth of the downflow can be made on the screen, and (ii) precise measurements of the density profiles in the stationary fluid environment by conductivity probe before and after each experimental run. Taking the difference between these profiles enabled the measurement of the net flow into or away from the environment of the downflow. The analysis procedure used to obtain this is described

in Baines (2001*a*, 2002) and briefly, is as follows. Taking the initial and final density profiles and differencing them gives the net change in vertical elevation of each density surface, as a result of the total inflow. From this, we may infer the total volume of fluid that has been sequestered below this density surface, as a result of this experiment. Dividing this by the run time gives a vertically continuous representation of the flux of fluid that has penetrated to below each density surface. Scaling this flux with Q_0 gives the function $\tilde{Q}(\rho)$. From $\tilde{Q}(\rho)$ we may calculate the net mean downward flow at a fixed height z from

$$Q(z) = Q_0 \int_{\rho_i(z)}^{\rho_f(z)} \tilde{Q}(\rho)\,\mathrm{d}\rho/(\rho_f(z) - \rho_i(z)), \tag{2.1}$$

$$\approx Q_0(\tilde{Q}(\rho_i(z)) + \tilde{Q}(\rho_f(z)))/2, \tag{2.2}$$

where $\rho_i(z)$ and $\rho_f(z)$ denote the initial and final density values at height z. Expressing this in terms of $Z = z/D$, we have

$$\hat{Q}(Z) = Q(z)/Q_0, \;\; Z = z/D. \tag{2.3}$$

$\hat{Q}(Z)$ is therefore an appropriately stretched version of $\tilde{Q}(\rho)$. The mean outflow velocity $v(z)$ from the downflow is then given by

$$v(z) = -\frac{dQ(z)}{dz}, \tag{2.4}$$

and in dimensionless form by

$$\hat{V}(Z) = v(z)D/Q_0 = -\frac{\mathrm{d}\hat{Q}(Z)}{\mathrm{d}Z}. \tag{2.5}$$

Examples of $\hat{V}(Z)$ are shown in the following section. Most results hereinafter are described in terms of the dimensionless vertical coordinate Z.

3. Observations

The values of the various parameters for the runs with bottom slopes of 20°, 25° and 30°, given in table 1, show that the initial values of the Buoyancy number B_0 cover approximately two orders of magnitude for each case, from ~ 0.001 to ~ 0.1. This covers the range of greatest variation in flow properties, and the transition between the flow regimes found for small and large (>0.1) B_0. One complication is that at the smallest values of B_0, the Reynolds number is also small (i.e. $Re = O(100)$), which means that viscous effects are significant in this limit, and the interpretation of these flows and their comparison with those at larger Re requires care. Qualitative descriptions of the mean flow have been obtained from careful observations of the videotapes of the movement of the fluorescein-dyed fluid, aided by the $\hat{V}(Z)$ curves. These are presented in the form of sketches in figures 2(*a*) to 5(*a*). Here the arrows denote mean motion, though the flow is often highly variable and turbulent, particularly in the mixing region above the bottom current. Values of the observed mean thickness of the bottom current near the upper part of the slope were measured on the screen, and these are given in table 1 for each run. The principal features of interest are the eventual distribution of the inflowing fluid, and the nature and location of the mixing processes that occur in causing this distribution. The results for a 30° slope are described first, because they most resemble the more familiar case of turbulent plumes. Flows for the smaller slope angles are then described in turn. Dynamical descriptions, models and interpretations are presented in the next three sections.

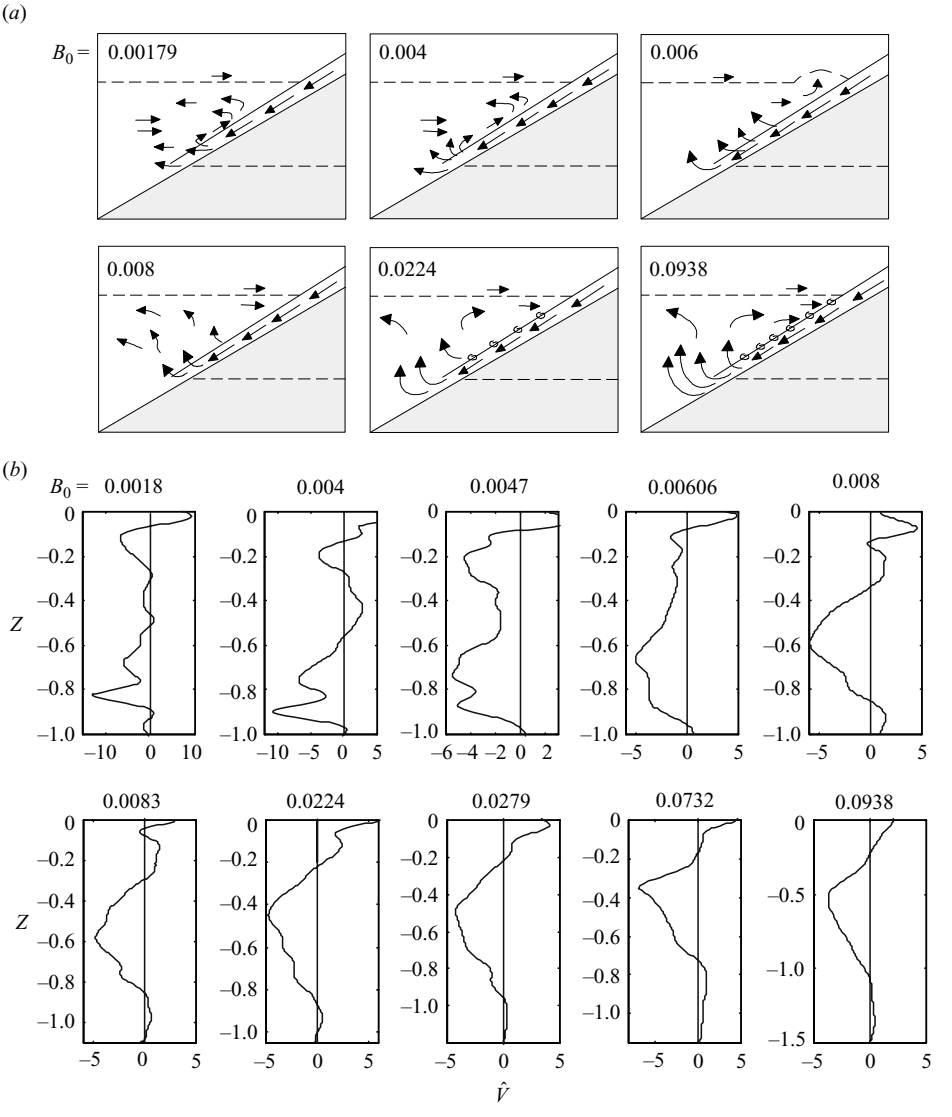

FIGURE 2. (*a*) Sketches of the observed flow for six representative values of B_0 for a slope angle of 30° slope with a smooth surface. These diagrams are indicative of the observed flow patterns, and are not intended to be quantitative. They have been constructed from examination of video tapes of the dye movements as viewed from the side, aided by the $\hat{V}$ curves shown in (*b*). In the region immediately above the bottom current, the flow is turbulent, and the arrows represent mean rather than steady motion. The upper dashed line denotes the upper limit of dyed fluid outside the initial downflow, which may be due to detrainment or springback. The lower dashed line denotes the initial equilibrium level of the dense fluid in the tank. As noted in the text, the first two runs are of a very unusual type, with two outflow regions separated by an entrainment region. (*b*) $\hat{V}$ profiles as a function of $Z = z/D$, for all the available runs for a slope angle of 30° with a smooth surface.

Figure 2(*a*) shows sketches of representative flow patterns for 30°. Corresponding $\hat{V}(Z)$ curves are shown in figure 2(*b*). The latter shows all available curves, whereas the former only shows six representative flow patterns. As figure 2(*a*) indicates, the flow patterns for all values of B_0 greater than about 0.006 bear a close resemblance to

the plume-type flow patterns described in Baines (2002). For these cases, the inflowing fluid enters as a turbulent gravity current with a highly convoluted upper boundary, where it mixes with the environment. This causes initial entrainment into the bottom current, as seen by the net inflow of the environmental fluid at the upper part of the water column. Most of this entrained fluid lies outside (above) the turbulent interface of the bottom current, but none the less, moves downslope with it. This entrainment continues down the slope until a point is reached where it decreases to zero. Beyond this point, the descending dense boundary fluid rises from the boundary in a large coordinated fashion, in a similar manner to that at the bottom of a (negatively buoyant) turbulent plume adjacent to a sidewall in a stratified environment (Baines 2002), as depicted in the bottom three frames of figure 2(*a*). One difference is that here, the region of separating motion appears to be more spread out along the slope, The rising motion, or 'springback', which is approximately steady in the mean, reaches up to a level that is $\sim 0.3D$ below the level of the inflow, below which it spreads laterally over a range of depths. Some of this fluid flows toward the wall where it is re-entrained into the bottom current, and the rest flows horizontally in the opposite direction, away from the wall. This is again the same behaviour that is seen in two-dimensional turbulent plumes. The $\hat{V}(Z)$curves for these values of B_0 are also notably similar to those in the bottom part of figure 7 of Baines (2002). There is one principal outflow region stemming from the springback process, with a single maximum, but with the suggestion of a second peak or 'shoulder' below. Above the dyed springback region, where $\hat{V} > 0$ near the top of the slope, there is entrainment of environmental fluid into the current. $\hat{V}$ is also positive below the outflow region (see figure 2*b*), and this latter region becomes more prominent and extends further below the level $Z = -1$ as B_0 increases. This is the overshoot region, in which the downflow overshoots the equilibrium level for the initial incident fluid, as seen for $B_0 = 0.0938$. Here, environmental fluid has been entrained into the turbulent boundary current, and then advected upwards in the springback process, causing a net inflow at these lowest levels of activity.

As the value of B_0 is decreased below 0.006 for 30° slopes, the pattern of flow changes. While there is still entrainment at the upper part of the slope as described above, the large-scale coordinated upwelling near the bottom of the downflow becomes less concentrated and energetic, and spreads upslope (see the upper right-hand frame in figure 2*a*, $B_0 = 0.006$). For values near 0.004, there is still a small amount of springback when this broad flow leaves the slope, but as B_0 further decreases it begins to resemble the broad detrainment region seen in downflows on gentle slopes (Baines 2001*a*). For the experiments with $B_0 < 0.005$, an unusual double-outflow was observed, as sketched in the first two frames of figure 2*a* and seen in the corresponding $\hat{V}(Z)$ profiles. An upper boundary to the dyed fluid, at a level near $Z = -0.1$, marks the upper boundary of the upper outflow region, which is the limit of the sprung-back fluid that has risen from below. Immediately below this level, there is a region of net outflow. Below this region in the video images there is a gap of clear fluid, except close to the boundary, implying that the fluid here is inflowing due to entrainment by the downflow; below this clear inflowing region is the main outflow region, filled with detrained dyed fluid. The fluid in the upper outflow region is in the entrainment region of the boundary current, so that this dyed fluid has come from the detraining region further down. The interpretation of this upper outflow is that this fluid has not been fully mixed with the main downflow, but was entrained into the outer parts of it. After detraining at the bottom, it rises past the intervening clear outflow region in a narrow and conspicuously turbulent region close to the entraining downflow, as schematically depicted in the first two frames of figure 2(*a*) ($B_0 = 0.0018$, 0.004).

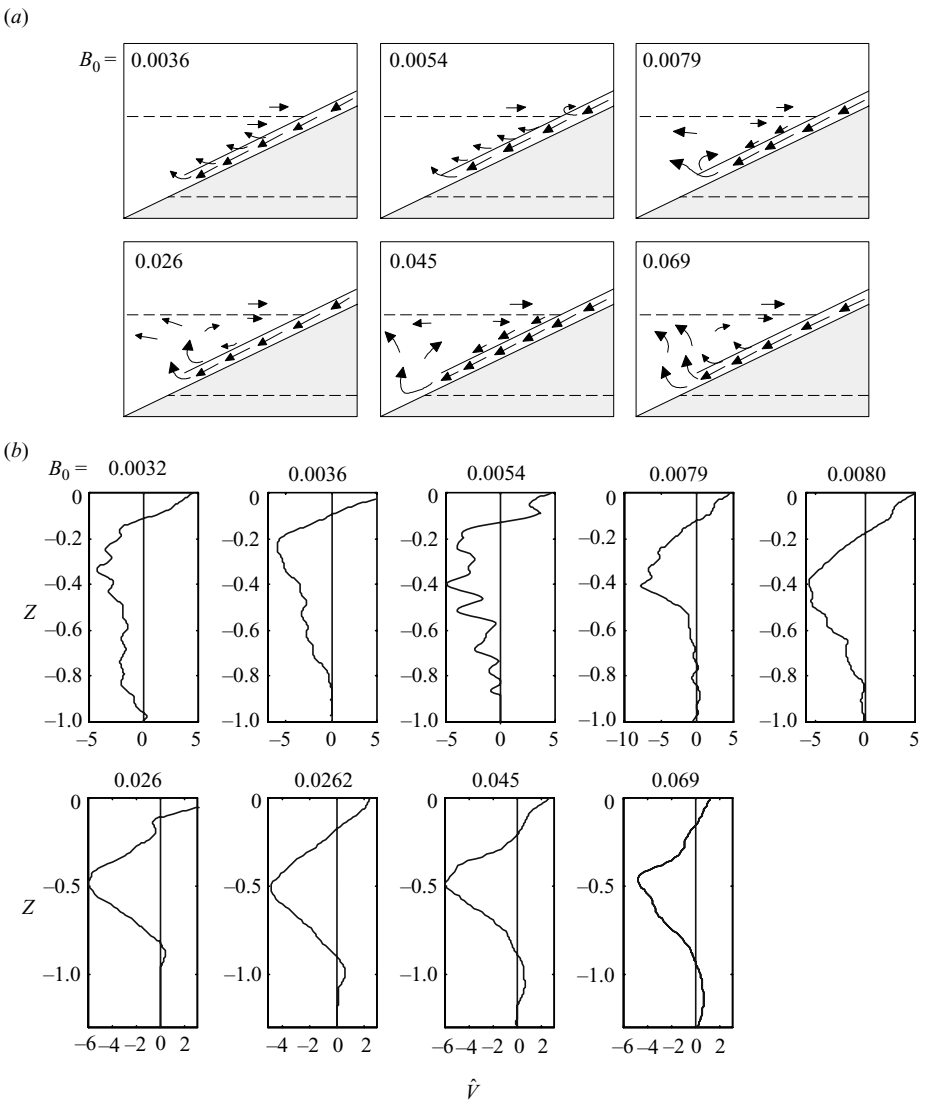

FIGURE 3. As for figure 2, but for a smooth slope of 25°.

As it passes, it is partly re-entrained, but sufficient fluid rises into the upper outflow region where the entrainment is weaker, and it is able to spread laterally away from the boundary. At the smallest values of B_0, this flow looks very different from the plume-type picture, but still does not resemble the gravity-current type observed on slopes of 12° and less; the picture here is complicated by the increased importance of viscous effects as represented by the low Reynolds numbers.†

The corresponding results for 25° slopes are shown in figure 3. For $B_0 > 0.01$, the flow has an essentially plume-like character, as for 90° slopes, with a large single outflow region and inflowing entrainment regions above and below. Large-scale overshoot and springback at the bottom are prominent. For $B_0 < 0.01$, the lower

† Videos of the various types of downflow including this unusual case, may be viewed on the web as a supplement to the online version of this paper or at http://www.bris.maths.ac.uk/~mapgb/.

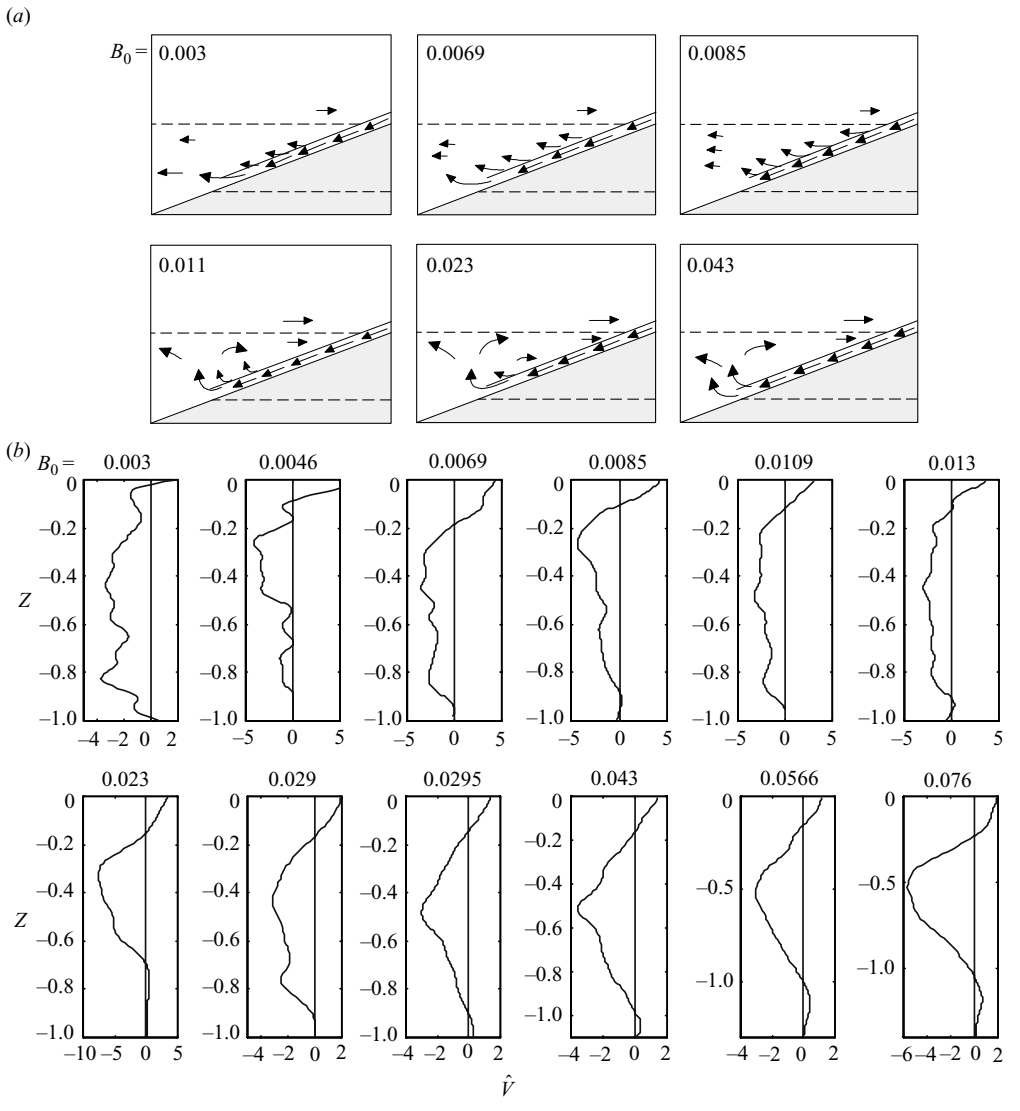

FIGURE 4. As for figure 2, but for a smooth slope of 20°.

entrainment region has virtually disappeared, and for runs with $B_0 < 0.007$ the flows more resemble the gravity current type, with a broad lower-level region of fluid leaving the vicinity of the boundary and flowing away from it, with a small degree of local rising motion as it does so. However, there is no lower maximum in outflow, implying that there is still considerable entrainment and small-scale springback in these low B_0 flows. No indication of the double outflow structure seen for 30° was seen for 25° slopes, or any of the others described here.

The results for smooth 20° slopes are shown in figure 4. Here the runs with $B_0 > 0.02$ are clearly of the plume type, and they more closely resemble the classic plumes for vertical slopes as B_0 increases further. For small B_0, the flows have some visual resemblance to gravity currents, with some detrainment along most of the downflow. However, as B_0 increases, the entrainment near the top of the slope increases, and the

Slope angle (deg.)	Type of surface	B_0 minimum value for plumes
12	Smooth	0.045 ($\pm$0.01)
20	Smooth	0.009 ($\pm$0.001)
20	Doormat	0.03 ($\pm$0.005)
25	Smooth	0.007 ($\pm$0.001)
30	Smooth	0.005 ($\pm$0.001)

TABLE 2. The dividing value of B_0 for differing slope angles, as inferred from the observations shown in figures 2–5. These values were obtained by classifying each run as P-type or GC-type, and the tabulated values divide the two sets in each series of experiments.

region of detrainment contracts toward the bottom of the downflow and shows some degree of small-scale springback, in which the fluid immediately rises a short distance on leaving the slope. As the value of B_0 approaches and exceeds 0.01, the region of 'detrainment' becomes concentrated at the bottom of the slope, giving a large and conspicuous region of rising fluid reminiscent of that at the bottom of a plume.

Some experiments were carried out with sandpaper (grain size $\sim$1 mm) on the bottom surface to explore the effect of an increase in roughness. This is marked by the symbol S_a, as distinct from S, in table 1, for the runs with $B_0 = 0.0085$ and 0.023. This was not observed to cause any significant difference to the results, compared with those for the smooth surfaces for neighbouring B_0 values. The same results were also obtained when the same sandpaper was attached to the sloping bottom for some 12° slopes, for a range of B_0 values which are not reported here – no significant change was observed with this increased roughness. In view of this, further experiments were carried out with very large roughness, namely a rubber doormat of common design with isolated roughness elements of a height of 7 mm that occupied approximately a quarter (measured to be 24 %) of the total volume below this level, a significant fraction of the thickness of the downflowing layer. These results are presented in figure 5. Here, the flow for small B_0 values is clearly of the gravity-current type, and closely resembles that observed for the small slope angles ($\leqslant$12°) in all respects. There is some entrainment at the very top of the slope, but over most of the length of the downflow the dense fluid detrains, giving a substantial outflow tongue at the bottom of the downflow, a short distance above the level of the density of the inflow. There is no springback of detrained fluid along the downflow, or at the bottom tongue. As B_0 is increased to values near 0.01, the outflow in this bottom tongue decreases in size, but the flow character remains unchanged with the exception that a small degree of springback is observed in the detrained fluid along the downflow. This flow type continues until B_0 exceeds values of about 0.03, above which the plume-like regime begins to become apparent, and this trend continues up to the maximum value examined, $B_0 = 0.084$.

For all of these slope angles, the flow at large B_0 values has the same character – that of turbulent plumes on a steep slope, with entrainment into the current over most of the length of the downflow, and a large region of springback at the bottom providing most if not all of the outflow. Some net entrainment and inflow into the plume occurs in the overshoot region at the bottom, but this is less conspicuous than with vertical slopes, and for corresponding B_0 values, the magnitude of this decreases with the slope angle. For each set of runs, an approximate lower limit of B_0 values for this plume-like behaviour may be identified, and estimated values of this are given in table 2. As B_0 decreases below this value, the bottom springback region begins

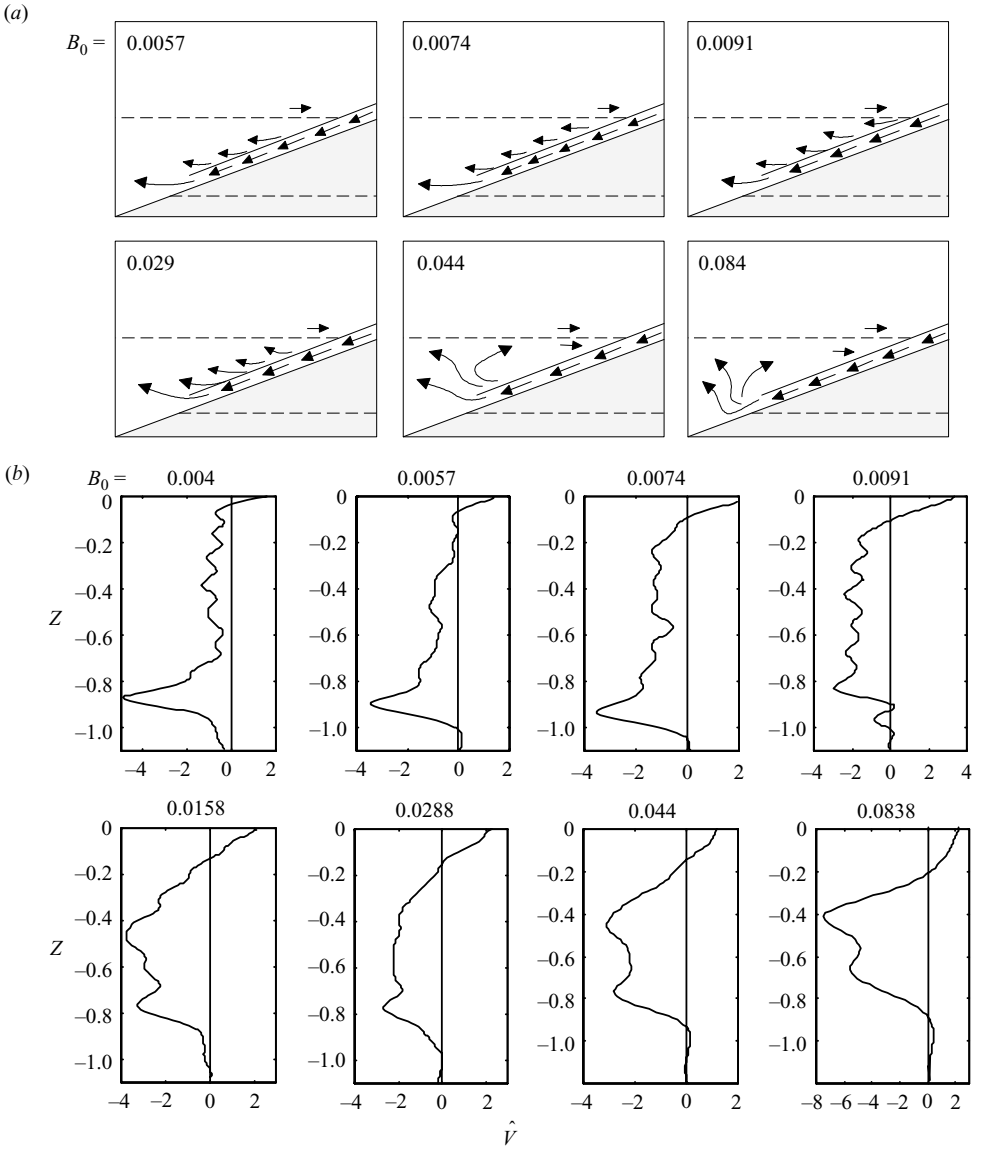

FIGURE 5. As for figure 2, but with a doormat surface (roughness elements 7 mm high) on a slope of 20°.

to spread upslope, with small-scale springback occurring along an increasing part of the downflow. This small-scale springback then decreases to zero, giving the differing flows seen at small B_0 for the different sets of runs, as described above. We note in passing that the three runs at 12° slope described in Baines (2001*a*) for which $B_0 > 0.06$ should now be classified as 'plumes', or P-type. The $\hat{V}$ curves for these runs are shown in figure 11 of Baines (2001*a*), and an examination of the corresponding video tapes shows the P-type pattern. This divide at 12° is also given in table 2.

I next describe the observed properties of these flows on each side of the divide of table 2 (the GC- and P-regimes), that relate to the observations on small and vertical slopes, respectively. For flows on the gravity-current-like side of the divide of table 2,

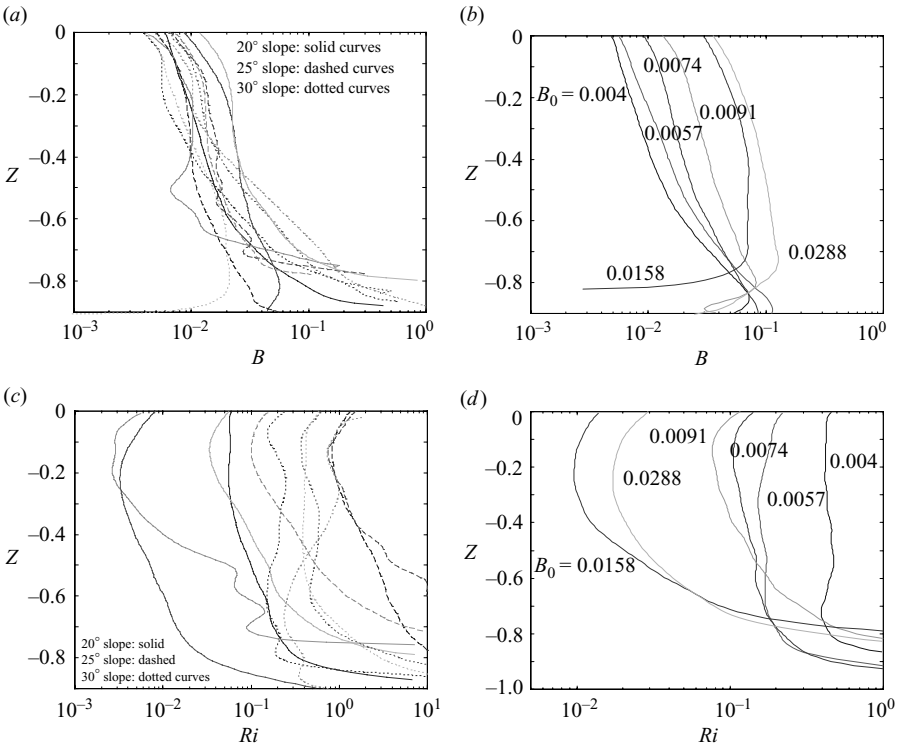

FIGURE 6. (*a*) Profiles of $B(Z)$ for runs on the gravity-current side of the divide of table 2, for flow over smooth surfaces with slope angles of 20°, 25° and 30°. (*b*) As for (*a*), but for doormat surface of 20°. (*c*) As for (*a*) but for Richardson number profiles $Ri(Z)$. (*d*) As for (*b*), but for Richardson number profiles $Ri(Z)$.

the profiles of B and Ri with height are shown in figure 6. These may be compared with the corresponding curves for gentler slopes in figure 13 of Baines (2001*a*). For the $B(Z)$ curves of figure 6(*a*) and 6(*b*), there is a tendency for B to increase with downslope distance, but this is not as marked as for the smaller slopes. This gradient also tends to increase with increasing B_0, but reverses as the boundary with the plume regime is approached. The 'doormat' curves of figure 6(*b*) show this trend more clearly. The Richardson number curves for the gentle slopes show decreasing values of Ri with increasing downslope distance for small slopes, but this decreases to near zero gradients for 6° slopes, and reversed sign for 12° slopes, where there is an increase. This latter behaviour (Ri increasing with $|Z|$) is also seen for the 20°, 25° and 30° slopes, for both smooth and doormat surfaces (figures 6*c* and 6*d*), and becomes more pronounced as B_0 increases. Although there is more scatter at these steeper slopes, the pattern is generally consistent with the trend in behaviour from 3° to 12° slopes, for both the $B(Z)$ and $Ri(Z)$ curves.

Quantitative observations of the properties of the flows on the 'plume-like' side of the divide of table 2 are shown in figure 7, which shows the same variables as calculated for vertical plumes by Baines (2002, figure 8). Z_1, Z_2, and Z_3 give the values of the zero crossings of the $\hat{V}$ curves, where Z_1 denotes the upper limit of the outflowing fluid from the process of springback, Z_2 the lower limit, and Z_3 the point of furthest extent of the downflow as measured by the entrainment. $\hat{Q}(Z_1)$ and $\hat{Q}(Z_2)$ are the net downward mass flux at these levels, and $\hat{Q}(Z_3) = 0$ by definition.

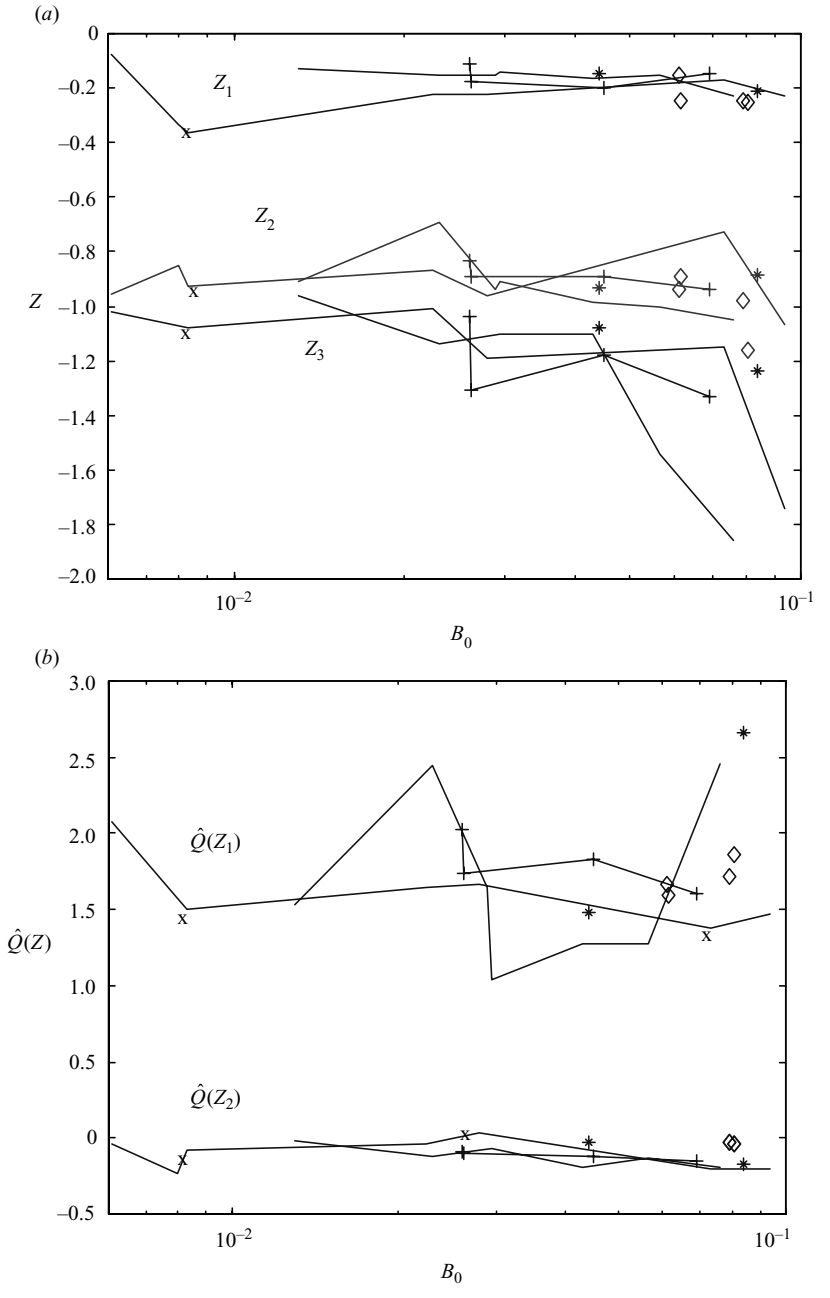

FIGURE 7. (*a*) Observed values of the variables Z_1, Z_2 and Z_3 for flows on the plume side of the divide in table 2, for all slopes from 12° to 30°. These variables denote zero crossings of the $\hat{V}$ curves. Z_1 and Z_2 denote the upper and lower limits of the outflowing fluid as a result of the springback process, and Z_3 denotes the furthest extent of the downflow, as observed from entrainment. The symbols here denote: ◇, 12° slope; *, 20° slope, doormat surface, both without lines. The three lines connect points for the smooth 20° slope (no symbols), for the 25° slope (+) and for the 30° slope (×). (*b*) Observed values of $\hat{Q}(Z_1)$ and $\hat{Q}(Z_2)$ for the P-type runs. The symbols have the same meaning as for (*a*).

For vertical plumes, the values of Z_1, Z_2 and Z_3 all showed a decrease with increasing B_0, particularly for Z_2 and Z_3. Here, the Z_1 and Z_2 values are effectively constant. Z_3 shows a decreasing trend for slope angles 20°, 25° and 30°, though there is considerable scatter, particularly for 20° slope data. $\hat{Q}(Z_2)$ gives a measure of the quantity of fluid that is entrained at the bottom of the plume, and lifted to higher levels in the outflow. The values here are approximately uniform in B_0 with a mean value of approximately −0.1 for all of these slope angles. This is smaller than those for vertical plumes (−0.4). The values of $\hat{Q}(Z_2)$ for 12° slopes are very small, and corresponding Z_3 values are not measurable. The $\hat{Q}(Z_1)$ values show considerable scatter with no discernible trend, and are also less than those for vertical plumes. Hence, despite the scatter and relatively small number of samples in the data, these properties support the notion that these flows may be identified as plumes, and modelled as such. This is quantitatively tested in the next section.

4. The plume model and P-regime observations

This plume-like regime is best represented by flow of dense fluid from a continuous line-source that descends vertically into a stratified fluid, under gravity (Baines 2002). The presence of a vertical wall is almost incidental except that it provides some frictional drag and supresses meanders (Kotsovinos & List 1977), but otherwise it does not affect the main character of the flow. The downward buoyancy is the dominant force on the dense inflow, and consequently the momentum flux increases downward. Turbulent mixing associated with the shear at the boundary of the downflow causes environmental fluid to be entrained into it, so that the net volume flux continually increases with downward distance. This process continues beyond the point where the buoyancy force vanishes and then becomes negative: the downward momentum of the plume carries it to a point where the velocity vanishes (the termination point). The fluid in the plume then moves away from the wall and rises with little mixing to spread across a range of heights appropriate to the range of density within it (the 'springback process'). Comparison with experiments (Morton, Taylor & Turner 1956; Bloomfield & Kerr 1998; Baines 2002) shows that the qualitative behaviour at least is reasonably well described by bulk equations for the volume, buoyancy and momentum fluxes in the plume.

This model may be generalized to flow down slopes that are not vertical. For two-dimensional flows down slopes that are steep enough to be dominated by these factors of buoyancy and entrainment, the bulk equations are

$$\frac{\mathrm{d}Q}{\mathrm{d}s} = EU = EQ/\bar{d}, \tag{4.1}$$

$$\frac{\mathrm{d}(Q^2/\bar{d})}{\mathrm{d}s} = S_2 G\bar{d}\sin\theta - C_D U^2 = S_2 G\bar{d}\sin\theta - C_D Q^2/\bar{d}^2, \tag{4.2}$$

$$\frac{\mathrm{d}G}{\mathrm{d}s} = -N^2\sin\theta - \frac{EG}{\bar{d}}, \tag{4.3}$$

where the notation is mostly defined in §1. The volume flux in the downslope s-direction is $Q = U\bar{d}$, where U is the mean fluid velocity in the plume, $\bar{d}$ is its width, and E is the entrainment coefficient. C_D is the drag coefficient; for these experiments, a suitable value is taken to be 0.006 for smooth surfaces, and 0.013 for the rough 'doormat' surface. These equations are essentially those of Ellison & Turner (1959), with the variable buoyancy of the environment added. Experimentally determined values of S_2 range from 0.6 to 0.9, and we here take a mean value of 0.75. It is customary (Turner 1986) to omit the pressure gradient term in (4.2), and this has

been done here. For flow on non-vertical sloping surfaces, a hydrostatic form of this term could be included, adding a term $-S_1(\mathrm{d}/\mathrm{d}s)(\bar{d}^2 G\cos\theta/2)$, where the shape factor (Ellison & Turner 1959) $S_1 \approx 0.2$ to the right-hand side of (4.2). This term is small on steep slopes, but may be significant on gentler slopes and is included in the gravity-current model outlined in § 5. However, its inclusion in this plume model makes the solutions less realistic and more difficult to interpret, and hence is omitted here.

If we define the Richardson number $Ri = G\bar{d}^3\cos\theta/Q^2$, the momentum equation may be replaced by an equation for $\bar{d}$, namely

$$\frac{\mathrm{d}\bar{d}}{\mathrm{d}s} = 2E + C_D - S_2\, Ri\tan\theta, \tag{4.4}$$

so that (4.1), (4.3) and (4.4) give the required equations for Q, G and $\bar{d}$. Substituting $\theta = \pi/2$ gives the equations for vertical plumes (Baines 2002). For present purposes, we call this the P-regime. It should be emphasized that, in this flow type and as described by this model, the downflow entrains over most of its path. The fluid entering the environment comes from the end of this downflowing current. The model does not describe the subsequent springback and entry of the fluid into the environment, and any mixing that is associated with this process. The entrainment coefficient for these flows is assumed to be a function of the Richardson number, and a number of functional forms have been fitted to various observations of entrainment in stratified shear flows (Fernando 1991). For practical purposes, many of these are equivalent, and we here choose a form inferred for downslope flows into homogeneous environments from Ellison & Turner (1959), as modified by Turner (1986), namely

$$\left.\begin{array}{ll} E = 0.08, & Ri < 0, \\ E = \dfrac{0.08 - 0.1Ri}{1 + 5Ri}, & 0 < Ri < 0.8, \\ E = 0, & Ri > 0.8. \end{array}\right\} \tag{4.5}$$

We may compare some predictions from this model with observations, as was done for vertical plumes in Baines (2002). For the initial conditions at the top of the slope, we take $(Q(0), G(0), \bar{d}(0)) = (Q_0, G_0, 1)$, with the gap height of 1 cm taken as the initial thickness. Z_f is the theoretical endpoint of the downflow, where the downward velocity U vanishes, and this may be compared with Z_3, and the level of the peak of the model outflow Z_m, defined by

$$Z_m = Z_f - \hat{G}_f,$$

may be compared with the level of the peak of the observed outflow, Z_{out}. This is based on the assumption that, if $\hat{G}_f$ denotes the buoyancy of the fluid at the bottom of the downflow in the model, and little mixing occurs in the large-scale springback process, the fluid leaving the downflow should gravitate to level Z_m. This comparison is shown in figure 8, using the small number of P-type points for each slope angle from 12° to 30°. The theoretical curves for Z_m and Z_f are similar for all slope angles 20°, 25° and 30°. The comparison is hampered by the degree of scatter and the small number of each set of points, but does indicate that there is some consistency between Z_f and Z_3, though there is considerably less between Z_m and Z_{out}. The theoretical values Z_f lie slightly above most of those for Z_3; there is some discrepancy at large B_0, but the three large values for Z_3 may not be significant, because the associated values of $\hat{Q}(Z_2)$ are small. The theoretical values for $\hat{Q}(Z_1)$ (not shown), the flux at the lowest level not influenced by springback, are also consistent with observations,

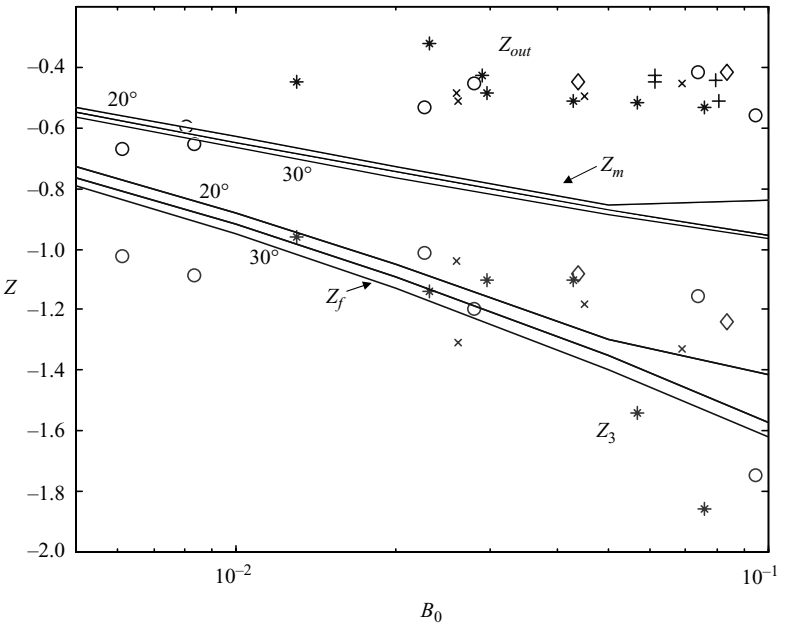

FIGURE 8. Comparison between the observed values Z_3 and Z_m for all plume-like flows with the corresponding theoretical values Z_f and Z_{out}, computed for smooth slopes with slope angles of 20° to 30°. The symbols here denote: +, 12° slope; *, 20° smooth slope; ◇, 20° doormat slope; ×, 25° slope; ○, 30° slope.

but mostly lie slightly below those shown in figure 7(*b*). This model can probably be improved by judicious tuning, but there are obvious limitations to a model that assumes that the fluid in the plume is locally homogeneous. No further quantitative use of this model is made in this discussion here. The main purpose of this section is to demonstrate that the flows in this P-regime for these slope angles may be modelled qualitatively as plumes; however, the comparison with observations is less than satisfactory, and more detailed models are probably required for quantitative results.

The dynamics of these flows depend on the strength of the (negative) buoyancy of the fluid in the current, increasing the momentum flux as the fluid moves downstream, causing mixing and entrainment. If buoyancy becomes small enough so that the surface drag force is comparable, momentum flux remains constant, the flow rate, mixing and entrainment are reduced, and the model breaks down. This becomes more pronounced for smaller $\bar{d}$.

5. The gravity current model and GC-regime observations

Downflows in this gravity-current-like regime are characterized by entrainment into the downflow at a rate E_eU, and detrainment from it at a rate E_dU (Baines 1999, 2001a). Note that here the downflow has a distinct upper interface, and this entrainment and detrainment (and their coefficients) refer to the transfer of fluid across this interface. This concept of entrainment is therefore different from that for plumes described in the previous section, where it refers to the net inflow toward the plume. The corresponding equations may be written (Baines 2001*a*)

$$\frac{\mathrm{d}Q}{\mathrm{d}s} = (E_e - E_d)\frac{Q}{\bar{d}}, \tag{5.1}$$

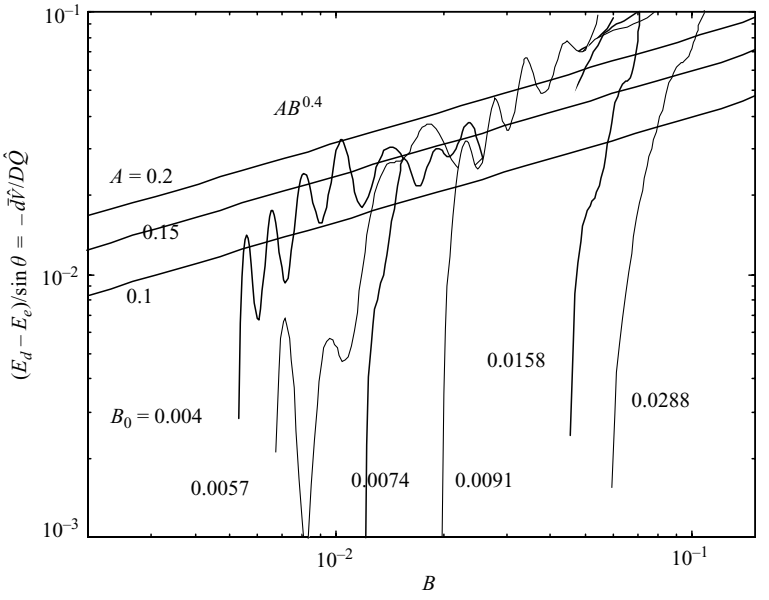

FIGURE 9. The function $(E_d - E_e)/\sin\theta = -d\hat{V}/D\hat{Q}$, evaluated from (5.1) in the form (5.5), plotted as a function of B, for the 20° doormat runs on the gravity-current side of the divide of table 2. The empirically determined form $AB^{0.4}$ from Baines (2001) is also plotted, for A values of 0.1, 0.15 and 0.2.

$$\frac{\mathrm{d}G}{\mathrm{d}s} = -N^2 \sin\theta - E_e G/\bar{d}, \tag{5.2}$$

$$(1 - Ri\cos\theta)\frac{\mathrm{d}\bar{d}}{\mathrm{d}s} = 2E_e + C_D - E_d - Ri\big(\sin\theta + \tfrac{1}{2}E_e\cos\theta + \tfrac{1}{2}\sin\theta(RiB^2\cos^2\theta)^{1/3}\big), \tag{5.3}$$

where

$$E_e = \frac{C_1(\theta)}{R_i}, \quad E_d = \frac{C_1(\theta)}{Ri} + 0.2B^{0.4}\sin\theta. \tag{5.4}$$

These expressions for E_d and E_e have been determined from experiments with slope angles of up to 12°. An observationally determined form for $C_1(\theta)$ for small slope angles is given in Baines (2001*a*). For these flows, there is an approximate dynamical balance between buoyancy and net drag, so that there is no overshoot at the bottom. The inflowing fluid does not penetrate beyond the equilibrium level of its initial density.

The question arises as to how well the expressions (5.4) for E_d and E_e apply to flows with slope angles up to 30°. For the above model, from (5.1), $E_d - E_e$ is given by

$$E_d - E_e = -\frac{\bar{d}\sin\theta\hat{V}}{\hat{Q}D}, \tag{5.5}$$

and all of the properties on the right-hand side may be determined from observations. The results for the 'doormat' runs on the gravity current side of the observed 'divide' are shown in figure 9. For these flows, the greatest similarity with flows at small slope angles is found at small B_0, furthest from the GC–plumes divide. We note, however,

that here the coefficient of $E_d - E_e$ appears closer to 0.15 than 0.2, as given in (5.4). (There are conspicuous oscillations in these curves which are also found in the observations at small slope angles, and are attributed to columnar disturbance modes, but these are not important for the present discussion.) This power law form breaks down as B_0 increases to values greater than 0.01, approaching the GC–P boundary of table 2. For the smooth surfaces of 20°, 25° and 30°, there is considerable scatter in the data for $E_d - E_e$ (not shown here), which is a reflection of the fact that many of these flows are not pure gravity currents as described for small slopes. However, despite the large variability, there is a general tendency for these curves to be concentrated near the power relationship of (5.4). As for the doormat, the departure of the observed values from this theoretical curve increases as B_0 increases and conditions approach the regime boundary with plumes. In summary, despite the variability and the small number of samples for each slope angle, there is a general consistency between $E_d - E_e$ as given in (5.4) and these observations over the range of depths where detrainment occurs, i.e. between the initial entrainment at the top of the slope, and the intrusion region at the bottom. We will assume its applicability in the following discussion for both smooth and rough surfaces.

The above form for E_e may be assumed to apply for Ri values down to about 0.1, but is not suitable for very small Ri. There is experimental evidence (Fernando 1991; Strang & Fernando 2001) that E_e for entrainment across a density interface in a shear flow becomes constant as $Ri \to 0$. This suggests taking

$$\left.\begin{aligned} E_e &= \frac{C_1(\theta)}{0.1}, \quad 0 < Ri < 0.1, \\ E_e &= \frac{C_1(\theta)}{Ri}, \quad Ri > 0.1. \end{aligned}\right\} \tag{5.6}$$

The 'junction value' of 0.1 is somewhat arbitrary, and this form should be regarded as approximate for small Ri. The precise value of E_e is not important if it is small. What is important is to avoid the non-physical singularity at $Ri = 0$, and this form is used in the remainder of this paper. The form of $C_1(\theta)$ has not been measured for slope angles greater than 12°, and a constant value of 1.2×10^{-4} will be assumed here. Note also that $\bar{d}$ has a slightly different interpretation in the plume and gravity-current regimes.

In the remainder of this paper, we discuss the parameter ranges where these flow types occur, and the locations of the boundaries between them.

6. Regime boundaries

In a typical experiment in the GC-regime, after steady downflow has become established, the incoming fluid at the top of the slope initially becomes turbulent as it moves downslope (for sufficiently large Reynolds number, Re). Here it entrains some environmental fluid as for homogeneous environments (Ellison & Turner 1959; Pawlak & Armi 2001). However, the character changes when the fluid travels sufficiently far to feel the stratification. Which of the two flow regimes that then becomes established depends on the balance of terms in the momentum equation. In the 'gravity current' regime, there is a balance between buoyancy and drag, $\bar{d}$ and Ri are approximately constant, and the right-hand side of (5.3) is near zero for a finite value of Ri. However, if the right-hand side becomes negative, $\bar{d}$ and Ri decrease to zero and the gravity current model is no longer viable. Instead, the greater mixing that results from this more unstable situation sets up the 'plume' regime, in

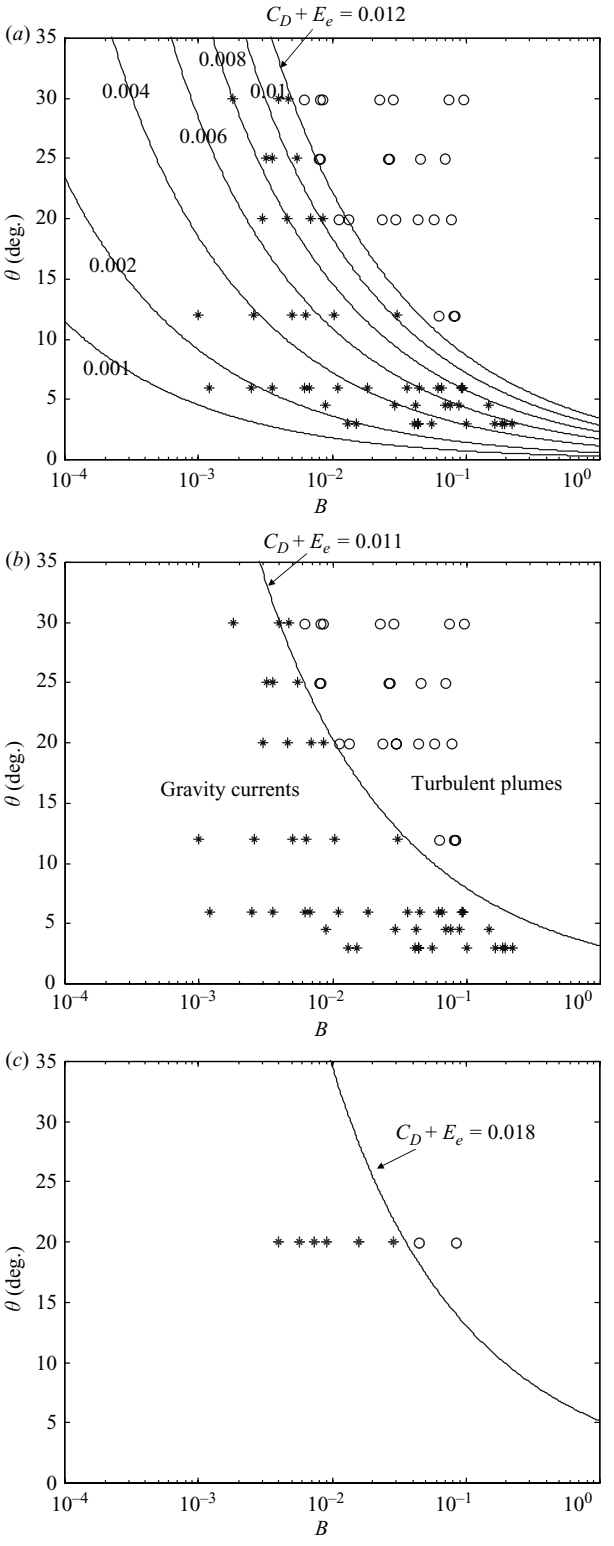

FIGURE 10. For caption see facing page.

which buoyancy dominates and accelerates the flow downward. Hence, for the gravity current model to be viable, the right-hand side of (5.3) should be non-negative, i.e.

$$2E_e + C_D - E_d - Ri\left(\sin\theta + \tfrac{1}{2}E_e\cos\theta + \tfrac{1}{2}\sin\theta(RiB^2\cos^2\theta)^{1/3}\right) \geqslant 0. \qquad (6.1)$$

This equality may be used to give an equilibrium value for Ri, but the limit of the model is reached when Ri and $\bar{d}$ approach zero, and this criterion then becomes

$$T \equiv C_D + E_e - 0.2B^{0.4}\sin\theta = 0. \qquad (6.2)$$

If $T < 0$, the GC model is no longer applicable. We may anticipate that when this barrier ($T = 0$) is crossed, the smallness of Ri and consequent increase in shear will cause greater instability, turbulence, mixing and entrainment, so that the plume model will become applicable. Curves for the criterion ($T = R_i = \bar{d} = 0$) in θ–B space are shown in figure 10(a) for various values of $C_D + E_e$, superimposed on all the data points for the various runs for smooth surfaces. Data for the experiments for vertical slopes (90°) are not included, but all of these flows are plumes, and the B_0 values range down to 0.0018. The plume dynamics become preferred as the slope becomes steeper, as B increases, and the drag coefficient decreases. For smooth surfaces, a good fit to this boundary between the two regimes is given by $C_D + E_e = 0.011$, as shown in figure 10(b). For the doormat runs, however, the boundary is at $C_D + E_e = 0.018$, reflecting the larger drag coefficient (figure 10c). Hence, the plume-type flows are observed in the parameter ranges where the GC-model cannot apply. This general consistency between these observed boundaries and the model criterion gives confidence in this interpretation of these results.

7. Conclusions and discussion

Flows down slopes into stratified environments may take two forms – a gravity-current-like regime (termed GC), and a plume-like regime (termed P). In the GC regime there is a balance between buoyancy and drag, so that the downflow consists primarily of an approximately locally homogeneous dense layer of constant thickness with a distinct upper interface, resembling a gravity current on a horizontal surface. This current entrains a small amount of fluid into it, but the mixing events that occur near its upper boundary over most of its length result in the stronger process of detrainment, in which mixed fluid leaves the vicinity of the downflow to find its own level in the environment. In the mean, this results in a continuous loss of fluid down the length of the current. In contrast, the P-regime resembles a turbulent plume, where the bottom drag is relatively less important, and the buoyancy force in the current is primarily balanced by mixing with the overlying environmental fluid. This strong mixing causes a net entrainment into the downflow, implying flow of the environmental fluid toward it along its length. The fluid in this plume overshoots its equilibrium density level, and springs back upwards in a large-scale motion with little associated mixing, to spread out over a range of heights of neutral density.

FIGURE 10. (a) Theoretical curves for the divide between gravity currents and plumes on the (B, θ)-plane as given by (6.2), for various values of $C_D + E_e$. All of the experimental points from smooth surfaces are also shown, with asterisks denoting gravity currents and circles denoting plumes. (b) As for (a), but showing the single value $C_D + E_e = 0.011$. (c) As for (b), but showing the single value $C_D + E_e = 0.018$, together with the points for the doormat surface at 20°.

On the basis of the experiments reported here and in Baines (2001*a*, 2002), the boundary in parameter space between these two regimes is given approximately by (6.2) which is derived as the limit of viability of the model describing flow in the GC-regime. The GC-regime may be found when $T > 0$, which may be due to large drag coefficient, small B or small slope angle. When $T < 0$, the GC-model is invalid, and the experiments over a wide range of slope angles from 12° to 90° indicate that the flow has turbulent plume character. Hence $T = 0$ may be regarded as marking the onset of the P-regime, and the flow properties are approximately described by a modified version of the conventional 'plume' model. It is possible that transitions may occur between the GC-regime and the P-regime on a downflow. This has not been conspicuous in any of these experiments, but may well occur on a long slope where the slope angle varies with downslope distance.

Some properties of the buoyancy number $B = QN^3/G^2$ should be noted in this regard. We observe that the limit $N \to 0$ implies $B \to 0$, which from (6.2) implies that gravity currents are found in this limit, although experiments give plumes (Ellison & Turner 1959). The reason for this is that, with Q and G held constant, the limit $N \to 0$ implies that $D \to \infty$, so that the theoretical endpoint of the downflow recedes down the slope to infinity. On the upper part of the slope in all these experiments, the flow is initially plume-like and entrains in a vertical distance that varies from $0.1D$ to $0.3D$, which correspondingly expands downslope as N decreases. Hence, at a fixed distance from the source region, decreasing environmental stratification tends to promote plume-like flow because the required distance for the fluid to travel to feel the effects of the stratification increases to large values beyond the field of view.

What is the main reason why the plume type flows entrain, but the gravity-current flows primarily detrain? The answer is dependent on the relative frequency of the turbulent mixing events that occur above the downflow. On a gentle slope, where buoyancy and bottom drag are approximately in balance, mixing events near the upper interface are sparse and relatively infrequent. A mixing event (due, say, to a breaking Holmboe wave – see §4.8.2 of Baines 1995) produces a patch of partially mixed fluid just above the interface, outside the downflow. Since, because of its isolation, there are no other factors affecting its motion, this patch is free to sink slowly under gravity to find its equilibrium level. This event results in net detrainment from the environment of the current. If the mixing events are more frequent so that the mixing events are not isolated, then it is possible that the flow above the interface may become organized into a three-dimensional pattern that does not affect the interface, and still results in detrained fluid leaving the environment of the boundary. Such a flow pattern has been observed and described by Mitsudera & Baines (1994), for flow over a slope of 6°, in the same tank as used here. In those observations, the spanwise pattern of the three-dimensional flow occupied the whole width (23 cm) of the working section, with outflow in the centre and some weaker return flow near the sidewalls. The experiment was repeated in a tank of width 150 cm, with the same parameter values (Q_0, G_0 etc.) per unit width. This resulted in approximately six periodic spanwise cells in the circulation above the downflow with similar width to that in the narrower tank, giving the same net detrained circulation. Hence, apparently coincidentally, the width of the narrow tank was sufficient to permit one cell.

If the slope is made steeper, or the drag coefficient is reduced, yet more mixing events occur at the upper boundary. If these become sufficiently frequent, they result in a broad sheet of partially mixed fluid, made up of closely spaced mixing events. In this situation, each parcel of mixed fluid is not sufficiently isolated to be able to

leave the slope. Instead, the collective effect of these parcels causes them to act in a coherent manner, move downslope with the main current, and become identified with it. The net result is that the collective mixed patches result in net entrainment into the downflow at the levels where they occur, and the flow assumes the 'turbulent plume-like' structure. This is a manifestation of the well-known Coanda effect in fluid mechanics, in which a turbulent mixing boundary current hugs the boundary. There is clearly a reasonably distinct boundary between these two types of behaviour, as expressed by (6.2) and table 2.

The bulk of this work including the experiments was carried out at CSIRO Atmospheric Research, Aspendale. The author is most grateful for the assistance of David Murray in all aspects of the experiments. This paper was completed while the author held a visiting Professorship at Bristol University funded by the Leverhulme Trust.

REFERENCES

Baines, P. G. 1995 *Topographic Effects in Stratified Flows*. Cambridge University Press, 482 pp.

Baines, P. G. 1999 Downslope flows into stratified environments – structure and detrainment. In *Mixing and Dispersion in Stably Stratified Flows*, *Proc. 5th IMA Conf. on Stratified Flows* (ed. P. Davies), pp. 1–21. Clarendon.

Baines, P. G. 2001*a* Mixing in flows down gentle slopes into stratified environments. *J. Fluid Mech.* **443**, 237–270.

Baines, P. G. 2001*b* Regimes for flows down slopes into stratified environments. *Proc. Intl Symp. on Stratified Hydraulics*, ISEH and IAHR, Arizona State University, Tempe, AZ.

Baines, P. G. 2002 Two-dimensional plumes in stratified environments. *J. Fluid Mech.* **471**, 315–337.

Bloomfield, L. J. & Kerr, R. C. 1998 Turbulent fountains in a stratified fluid. *J. Fluid Mech.* **358**, 335–356.

Britter, R. E. & Linden, P. F. 1980 The motion of the front of a gravity current travelling down an incline. *J. Fluid Mech.* **99**, 532–543.

Ellison, T. H. & Turner, J. S. 1959 Turbulent entrainment in stratified flows. *J. Fluid Mech.* **6**, 423–448.

Fernando, H. J. S. 1991 Turbulent mixing in stratified fluids. *Annu. Rev. Fluid Mech.* **23**, 455–493.

Kotsovinos, N. E. & List, E. J. 1977 Plane turbulent buoyant jets. Part 1. Integral properties. *J. Fluid Mech.* **81**, 25–44.

Mitsudera, H. & Baines, P. G. 1994 Downslope gravity currents in a continuously stratified environment: a model of the Bass Strait outflow. *Proc. 11th Australasian Fluid Mech. Conf. Hobart, Australia*, pp. 1017–1020.

Morton, B. R., Taylor, G. I. & Turner, J. S. 1956 Turbulent gravitational convection from maintained and instantaneous sources. *Proc. R. Soc. Lond.* A **234**, 1–23.

Nielsen, M. H., Pratt, L. & Helfrich, K. 2004 Mixing and entrainment in hydraulically driven stratified sill flows. *J. Fluid Mech.* **515**, 415–443.

Pawlak, G. & Armi, L. 2001 Mixing and entrainment in developing stratified currents. *J. Fluid Mech.* **424**, 45–73.

Price, J. F. & Baringer, M. O. 1994 Outflows and deep water production by marginal seas. *Prog. Oceanogr.* **23**, 161–200.

Strang, E. J. & Fernando, H. J. S. 2001 Entrainment and mixing in stratified flows. *J. Fluid Mech.* **428**, 349–386.

Turner, J. S. 1973 *Buoyancy Effects in Fluids*. Cambridge University Press, 367 pp.

Turner, J. S. 1986 Turbulent entrainment: the development of the entrainment assumption, and its application to geophysical flows. *J. Fluid Mech.* **173**, 431–471.